

# Analysis of Effective Connectivity in Mobile Wireless Communications

J. David Haughs and Dongsoo S. Kim

## Abstract

his research demonstrates the effect of a deployed regions boundaries on the effective coverage of a mobile node. A nodes coverage area is not uniform throughout the entire deployed region. Assuming a uniform coverage can result in significant error in calculations. In this study, we analyze the behavior of a nodes coverage area as a function of its transmission range throughout the entire deployed region. Using this analysis, a mathematical model for effective coverage in mobile wireless communications is created. The mathematical model considers the effect of the deployed regions boundaries on the coverage area of a mobile node. Lastly, we present simulation results to verify the analytical model and to compare this model with that of a uniform coverage.

his research demonstrates the effect of a deployed regions boundaries on the effective coverage of a mobile node. A nodes coverage area is not uniform throughout the entire deployed region. Assuming a uniform coverage can result in significant error in calculations. In this study, we analyze the behavior of a nodes coverage area as a function of its transmission range throughout the entire deployed region. Using this analysis, a mathematical model for effective coverage in mobile wireless communications is created. The mathematical model considers the effect of the deployed regions boundaries on the coverage area of a mobile node. Lastly, we present simulation results to verify the analytical model and to compare this model with that of a uniform coverage.

## I. INTRODUCTION

Ad hoc wireless networks are formed by a group of wireless mobile nodes. The wireless nodes can be any sort of microprocessor device with the ability for wireless communication. By nature, a wireless ad hoc network lacks any fixed network infrastructure. Users are provided connectivity with unrestricted mobility due to the self-organizing, rapidly deployable architecture of wireless ad hoc networks.

Because a node in a wireless ad hoc network is connected with unrestricted mobility, the topology of the network is dynamic. Realistic mobility modeling becomes very critical for analyzing node behavior and network performance. Common mobility models are the random walk and random waypoint mobility models [1], [4], [5], [9].

The random walk mobility model was derived from the Brownian motion, which is a stochastic process that models random continuous motion [8]. In this model, a mobile node moves from its current location with a randomly selected speed in a randomly selected direction. The new speed and direction are both chosen from pre-defined ranges,  $[v_{\min}, v_{\max}]$  and  $[0, 2\pi)$ , respectively [5]. The new speed and direction are maintained for an arbitrary length of time randomly chosen from  $(0, t_{\max}]$ . At the end of the chosen time the node makes a memoryless decision of a new random speed and direction.

In the random waypoint mobility model, a mobile node chooses a random destination within the deployed area. With the destination chosen, the mobile node randomly chooses a speed at which to travel arbitrarily from  $[v_{\min}, v_{\max}]$ . Upon reaching the destination, a mobile node will pause for a random time before determining a new destination and speed. In the random waypoint model, mobile nodes have a tendency to concentrate to the middle of the deployment region [4], [13], [15], indicating that this model does not present a truly uniform node distribution.

Both mobility models presented above are used regularly in the simulation of wireless mobile nodes [7], [14], [6], [11], [15], [16]. In addition to choosing the appropriate mobility model, one must

This research was supported in part by the National Science Foundation under grant CCF-0514975.

J.D. Haughs (david.haugh@gm.com) is with General Motors, USA

D.S. Kim (dskim@iupui.edu) is with Electrical and Computer Engineering of Indiana Univ. Purdue Univ. Indianapolis, USA

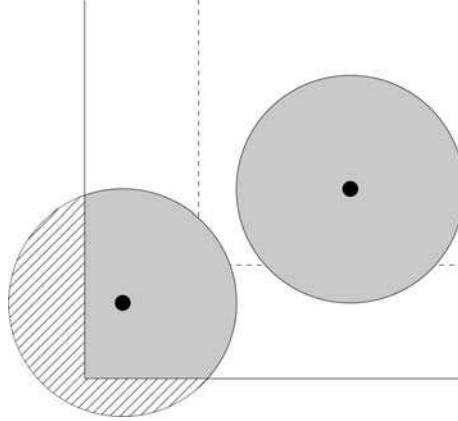


Fig. 1. Illustration of boundary effect using two identical nodes. One node's coverage extends beyond the boundary of the deployment region.

also understand the coverage of a MN under a given situation. It is common to assume a node has a uniform coverage area independent of its location within the deployment area without full understanding of the impact of the transmission range in that deployment area [3], [11]. This chapter will present the dependency of location and transmission power on the coverage of a MN and provide an analytical method for describing this behavior and analyzing connectivity of MNs.

## II. EFFECTIVE NODE COVERAGE

The effective coverage of a mobile node describes the number of MNs that can communicate with a given node in the deployment region. Effective coverage is dependent on the location of the node and its transmission power in relation to the size of the deployment region and nodal density.

For simplicity, it is assumed that a MN has a uniform circular transmission area that directly corresponds to its transmission power. The transmission power of a MN has a range of length  $r$  and can therefore be represented as the radius of the circular transmission area centered at the MN with a total transmission area of  $\pi r^2$ . This is commonly assumed but is not always true. As a MN moves about the deployment region, the transmission area could be affected by the boundary effect. The boundary effect occurs when a MN is at a distance less than  $r$  from one or more boundaries of the deployment region. At this distance a portion of the MN's total transmission area extends beyond the boundary of the deployment region. This portion of transmission area is considered unusable by the MN as there cannot exist a MN to communicate with beyond the boundary. Therefore, the effective coverage area of the affected MN is less than  $\pi r^2$ .

Figure 1 illustrates this behavior. The figure shows two identical nodes near one corner of a deployment region. The solid dot in the middle of the shaded circle is the MN, the shaded circle represents the transmission area of the MN. The dashed line in the figure is located a distance of  $r$  from the boundary. This line represents a threshold into a region of cutoff for a MN's effective coverage area. As can be seen in the figure, the MN that has crossed this threshold line and is nearing the boundary has a portion of its transmission area extending beyond the boundary of the deployment. This hatched area serves no benefit to the MN.

The boundary effect can have a major impact on the coverage area of a MN. When analyzing node connectivity in ad hoc networks it is important to take into account the boundary effect to prevent an overestimation of coverage area. Total transmission area data can be skewed by the cutoff areas at the boundaries.

## III. EFFECTIVE CONNECTIVITY MODEL

The purpose of this model is to predict node connectivity based on transmission range and to model the behavior of nodes under different simulations. An average effective connectivity area in two

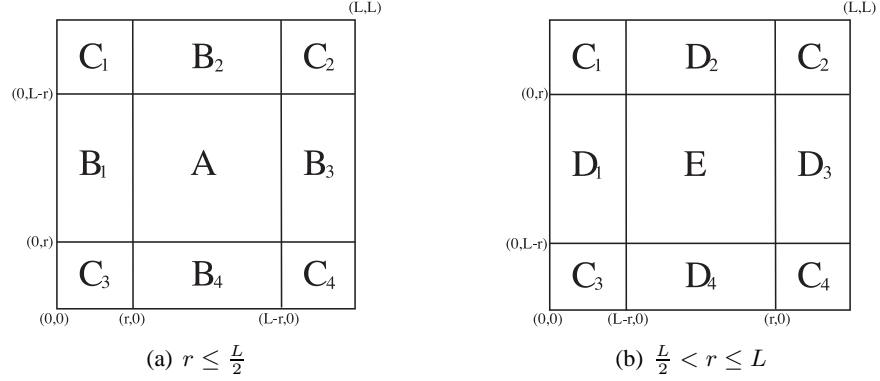


Fig. 2. Regional division of deployment area for computation of effective connectivity

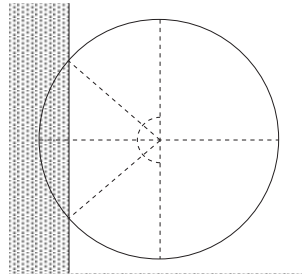


Fig. 3. Single edge boundary effect for a node within Region  $B_1$

dimensional space,  $\mu(r)$ , is given as

$$\mu(r) = \iint S(r, x, y) \times p(x, y) dx dy, \quad (1)$$

where  $x$  and  $y$  represent the location of the node,  $p(x, y)$  is the probability that a node is located at the point  $(x, y)$  and  $S(r, x, y)$  denotes the effective coverage of the node with the transmission range  $r$  and at the location  $(x, y)$ .

The analytical model is computed by considering a node's effective coverage area in different sections, or regions, of the deployment area. Figure 2(a) illustrates the regions in a  $L \times L$  deployment area when  $r \leq \frac{L}{2}$ . The regions are created based on the transmission range,  $r$ , of a MN. The distance  $r$  creates the various regions inside the deployment area. As  $r$  nears 0, region  $A$  will dominate the deployment, conversely as  $r$  nears  $\frac{L}{2}$ , regions  $C$  will dominate. For the case where  $\frac{L}{2} < r \leq L$  one must refer to Figure 2(b). As  $r$  increases beyond  $\frac{L}{2}$ , the lines representing the regions will cross paths and continue in opposite directions decreasing region  $C$  and creating two new regional divisions,  $D$  and  $E$ . All of the regions from  $A$  to  $E$  represent differing levels of effective coverage area and create different calculations for  $S(r, x, y)$ . The functions for  $S(r, x, y)$  for each region are explained in the following subsections.

#### A. Region A

Nodes lying within Region A do not have coverage areas intersecting any boundary and therefore, are able to utilize their entire coverage area. The coverage area of a node that is residing in Region A is given as

$$S_A(r, x, y) = \pi r^2 \quad (2)$$

#### B. Region B

In Region  $B$  a node's coverage area will extend beyond one and only one boundary of the deployment area. Figure 3 demonstrates this single edge boundary effect for a node within Region  $B_1$  of Figure 2.

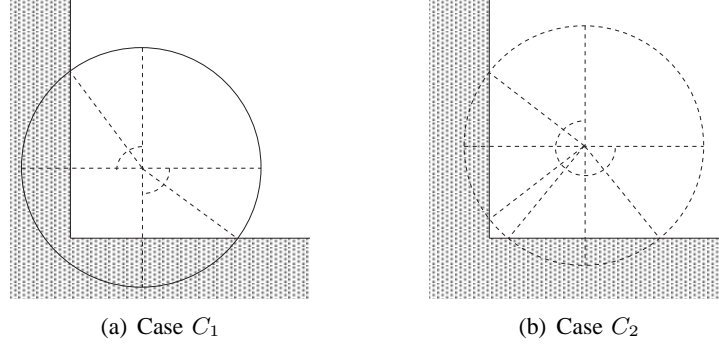


Fig. 4. Double edge boundary effect for a node within Region  $C_3$

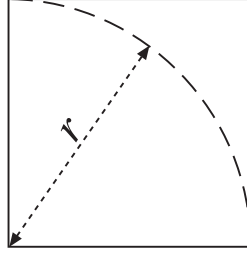


Fig. 5. Arc formed from  $r$  in region  $C_3$

It also shows how the effective area is broken into slices to obtain a function for effective coverage for a node within this region. For  $B_1$  the coverage area is

$$S_{B_1}(r, x, y) = x\sqrt{r^2 - x^2} + r^2 \left( \frac{\pi}{2} - \arccos \frac{x}{r} \right) + \frac{\pi r^2}{2} \quad (3)$$

Because  $B_1, B_2, B_3$  and  $B_4$  are symmetric Equation 3 can be used to represent each of the four regions of  $B$ . Therefore,

$$S_B(r, x, y) = S_{B_1}(r, x, y)$$

### C. Region C

The coverage area of a node within Region  $C$  will intersect two of the deployment area's boundaries. There are two cases to take into consideration for a node located in this region. The first case, shown in Figure 4(a) as Case  $C_1$ , occurs when a node is located no more than a distance of  $r$  from the corner of the deployment area. The second case, shown in Figure 4(b) as Case  $C_2$ , occurs when a node is located a distance greater than  $r$  from the corner but still within the bounds of region  $C$ . This distance  $r$  from the corner forms an arc inside of Region  $C$  as seen in Figure 5.

Within the region labeled  $C_3$  in Figure 2 the arc is defined as  $\sqrt{r^2 - x^2}$ . For a node located within  $C_3$  the first case of the coverage area for  $r \leq \frac{L}{2}$  is

$$S_{C_3}(r, x, y) = \frac{\pi r^2}{4} + \frac{1}{2}x\sqrt{r^2 - x^2} + \frac{r^2}{2} \left( \frac{\pi}{2} - \arccos \frac{x}{r} \right) + \frac{1}{2}y\sqrt{r^2 - y^2} + \frac{r^2}{2} \left( \frac{\pi}{2} - \arccos \frac{y}{r} \right) + xy \quad (4)$$

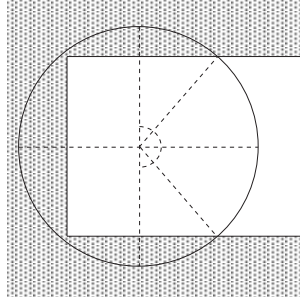


Fig. 6. Tripple edge boundary effect for a node within Region  $D_1$

The second case for  $r \leq \frac{L}{2}$  generates the equation

$$\begin{aligned}
 S_{C_3}(r, x, y) &= \frac{\pi r^2}{4} + \frac{1}{2}x\sqrt{r^2 - x^2} + \frac{r^2}{2} \left( \frac{\pi}{2} - \arccos \frac{x}{r} \right) + \frac{1}{2}y\sqrt{r^2 - y^2} \\
 &+ \frac{r^2}{2} \left( \frac{\pi}{2} - \arccos \frac{y}{r} \right) + \frac{1}{2}x\sqrt{r^2 - x^2} + \frac{1}{2}y\sqrt{r^2 - y^2} \\
 &+ \frac{r^2}{2} \left( \frac{\pi}{2} - \arccos \frac{x}{r} - \arccos \frac{y}{r} \right)
 \end{aligned} \tag{5}$$

As with  $S_B(r, x, y)$ , the regions of  $S_C(r, x, y)$  are symmetric. For the case of  $r > \frac{L}{2}$  within Region  $C$  shown in Figure 2(b) only the first of the above cases exists. For the effective connectivity in this region Equation 4 is used again, however the limits of integration will change when calculating  $\mu(r)$ .

#### D. Region D

Region  $D$  only exists when  $\frac{L}{2} < r < L$ . In this region a MN's coverage area intersects three of the deployment regions boundaries. Like Regions  $B$  and  $C$ , Region  $D$  is also symmetric. Figure 6 illustrates the coverage of a node within Region  $D$ . From this figure it can be seen that the coverage area of a node within this region is dependent on  $r$ ,  $x$  and  $y$  and the following equation can be obtained

$$\begin{aligned}
 S_{D_1}(r, x, y) &= xL + \frac{1}{2}(L - y)\sqrt{r^2 - (L - y)^2} \\
 &+ \frac{r^2}{2} \left( \pi - \arccos \frac{L - y}{r} - \arccos \frac{y}{r} \right) + \frac{1}{2}y\sqrt{r^2 - y^2}
 \end{aligned} \tag{6}$$

#### E. Region E

Region  $E$  emerges when  $\frac{L}{2} < r$  and continues to grow and take over the entire deployment region as  $r$  approaches  $L$ . The coverage area of nodes within Region  $E$  intersect the deployment region at all four boundaries. There are, however, four sub-cases to this region that are separated depending on the value of  $r$ . While it is true that all nodes within Region  $E$  will intersect all four boundaries of the deployment, they do so in different ways depending on location and transmission range.

The Figures 7(a) through 7(d) display the four sub-cases of Region  $E$ . In each of these figures the arcs represent the distance  $r$  from each of the four corners of the deployment region. The centralized square box represents Region  $E$  from Figure 2(b) bounded by  $L - r$  and  $r$  on both the  $x$  and  $y$  axis. As  $r$  increases the figures demonstrate the four sub-cases created as the arcs begin to overlap the centralized box and begin to further intersect themselves. These actions result in the four sub cases explained in the following subsections.

1) *Sub-case  $E_1$* :: Sub-case  $E_1$ , as shown in Figure 7(a), is valid for  $\frac{L}{2} < r \leq (2 - \sqrt{2})L$ .  $(2 - \sqrt{2})L$  is the point at which the arc of radius  $r$  meets the corner of the Region  $E$ . Nodes within this sub-case will expand beyond all four sides of the deployment region but will not overlap the corners of

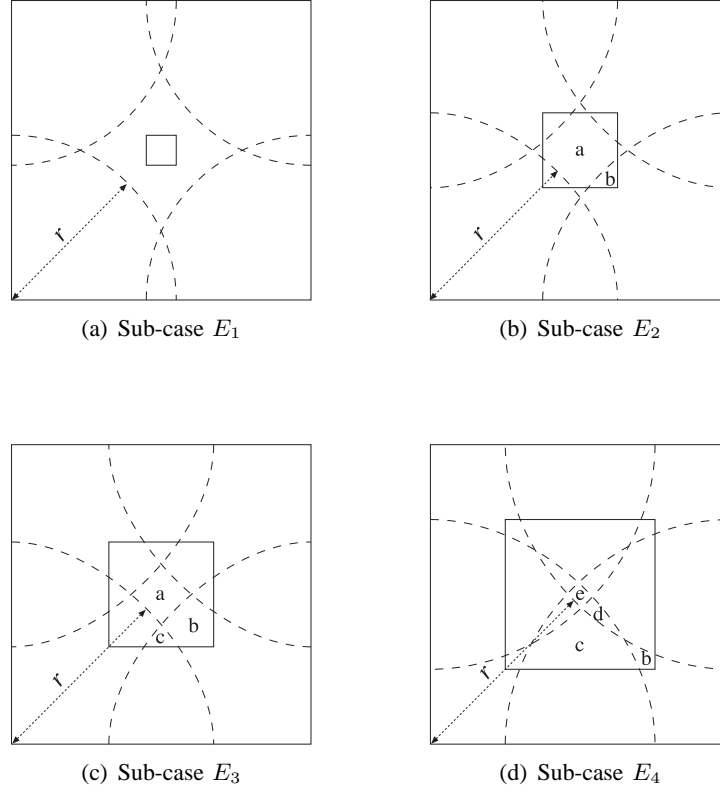


Fig. 7. Sub-cases for Region  $E$

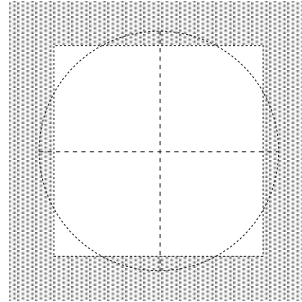


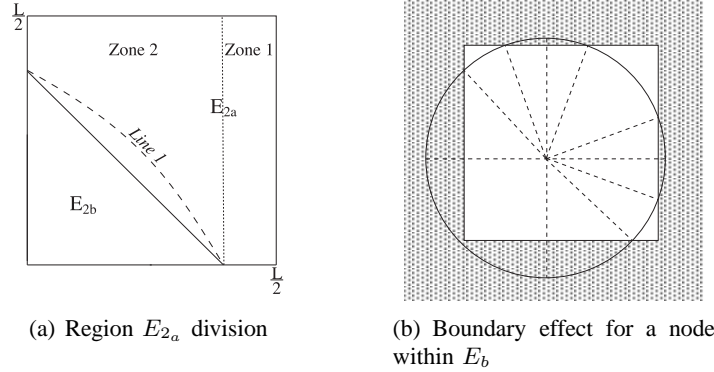
Fig. 8. Boundary effect for a node within  $E_a$

the deployment region as can be seen in Figure 8. Within the bounds of this sub-case the formula for coverage area within  $E_1$  is given as

$$\begin{aligned}
 S_{E_1}(r, x, y) = & \pi r^2 + x\sqrt{r^2 - x^2} + y\sqrt{r^2 - y^2} + (L - y)\sqrt{r^2 - (L - y)^2} \\
 & - r^2 \arccos\left(\frac{x}{r}\right) - r^2 \arccos\left(\frac{y}{r}\right) - r^2 \arccos\left(\frac{L - x}{r}\right) \\
 & - r^2 \arccos\left(\frac{L - y}{r}\right)
 \end{aligned} \tag{7}$$

2) *Sub-case  $E_2$* :: For sub-case  $E_2$ , the valid range for  $r$  is  $(2 - \sqrt{2})L < r \leq \frac{5}{8}L$ .  $\frac{5}{8}L$  is the point at which the intersection of the arcs meets the boundary of Region  $E$ . As shown in Figure 7(b), sub-case  $E_2$  is further broken into two sub-regions with separate calculations that are named  $E_{2_a}$  and  $E_{2_b}$ .

$$S_{E_2}(r, x, y) = S_{E_{2_a}}(r, x, y) + S_{E_{2_b}}(r, x, y)$$

Fig. 9. Sub-case  $E_2$ 

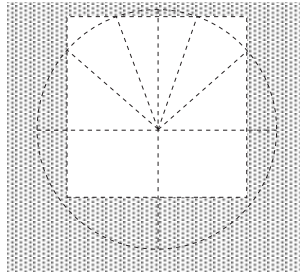
The breakup of Region  $E_{2a}$  is identical to that of sub-case  $E_1$  and is therefore calculated in the same manner but with different limits of integration. It was found that Region  $E_{2a}$  must be further subdivided into two zones to perform the calculation. The functions for zones are the same, however, they have different limits of integration. Figure 9(a) shows the lower left quarter of Region  $E$  from Figure 7(b) and how it is further divided into sub-regions and zones for calculations. To simplify the calculations the curved line labeled *Line 1* in Figure 9(a) is assumed to be a straight line with minimal error. The coverage area of a MN in these zones is

$$S_{E_{2a}}(r, x, y) = 4 \cdot S_{E_{2a_1}}(r, x, y) + 4 \cdot S_{E_{2a_2}}(r, x, y) \quad (8)$$

Nodes in  $E_{2b}$  again expand beyond all four sides of the deployment region, but also expand beyond one corner of the deployment region as can be seen in Figure 9(b). The representative equation for nodes within this region is given as

$$\begin{aligned} S_{E_{2b}}(r, x, y) = & \frac{\pi r^2}{2} + xy + \frac{x}{2} \sqrt{r^2 - x^2} + (L - y) \sqrt{r^2 - (L - y)^2} \\ & + (L - x) \sqrt{r^2 - (L - x)^2} + \frac{y}{2} \sqrt{r^2 - y^2} - \frac{r^2}{2} \arccos\left(\frac{x}{r}\right) \\ & - r^2 \arccos\left(\frac{L - y}{r}\right) - r^2 \arccos\left(\frac{L - x}{r}\right) - \frac{r^2}{2} \arccos\left(\frac{y}{r}\right) \end{aligned} \quad (9)$$

3) *Sub-case  $E_3$* :: Sub-case  $E_3$ , shown in Figure 10, is used when  $\frac{5}{8}L < r \leq \frac{L}{\sqrt{2}}$ . At the point that  $r = \frac{L}{\sqrt{2}}$  the arcs generated from opposing corners of the deployment region begin to overlap creating regions to be described in sub-case  $E_4$ . As one can see, sub-case  $E_3$  is broken into three sub-regions, consisting of three separate calculations, that have been named  $E_{3a}$ ,  $E_{3b}$  and  $E_{3c}$ . Region  $E_{3a}$ , like region  $E_{2a}$ , is similar to sub-case  $E_1$  and is therefore calculated the same, but with different limits of integration. Region  $E_{3b}$  is similar to that of  $E_{2b}$  in sub-case  $E_2$ . Nodes in the region represented by

Fig. 10. Boundary effect for a node within  $E_3$

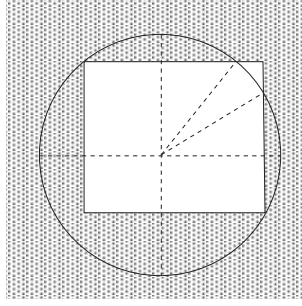


Fig. 11. Boundary effect for a node within  $E_4$

$E_{3_c}$  continue to overlap all four sides of the deployment area, but now they also overlap two of the four corners of the deployment area.  $E_{3_c}$  is calculated based on Figure 10 and is given as

$$\begin{aligned}
 S_{E_{3_c}}(r, x, y) &= \frac{\pi r^2}{2} + yL + \frac{x}{2} \sqrt{r^2 - x^2} + \frac{L-x}{2} \sqrt{r^2 - (L-x)^2} \\
 &\quad + (L-y) \sqrt{r^2 - (L-y)^2} - \frac{r^2}{2} \arccos\left(\frac{x}{r}\right) \\
 &\quad - r^2 \arccos\left(\frac{L-y}{r}\right) - r^2 \arccos\left(\frac{L-x}{r}\right)
 \end{aligned} \tag{10}$$

4) *Sub-case  $E_4$* : The final sub-case, sub-case  $E_4$ , shown in Figure 11 represents the case where  $\frac{L}{\sqrt{2}} < r \leq L$ . There are four sub-regions within sub-case  $E_4$  named  $E_{4_b}$ ,  $E_{4_c}$ ,  $E_{4_d}$  and  $E_{4_e}$ . The calculation for  $E_{4_b}$  is similar to that of sub-case  $E_{2_b}$  and the calculation for  $E_{4_c}$  is similar to that of sub-case  $E_{3_c}$ . Sub-case  $E_4$  presents two new sub-regions,  $E_{4_d}$  and  $E_{4_e}$ . Nodes within  $E_{4_d}$  are represented by Figure 11 and the equation for these nodes is given as

$$\begin{aligned}
 S_{E_{4_d}}(r, x, y) &= \frac{\pi r^2}{4} + yL + x(L-y) + \frac{L-y}{2} \sqrt{r^2 - (L-y)^2} \\
 &\quad + \frac{L-x}{2} \sqrt{r^2 - (L-x)^2} + \frac{r^2}{2} \arccos\left(\frac{L-y}{r}\right) \\
 &\quad + \frac{r^2}{2} \arccos\left(\frac{L-x}{r}\right)
 \end{aligned} \tag{11}$$

Sub-region  $E_{4_e}$  is the case in which a node's coverage area expands beyond the entire deployment region and is therefore equal to the area of the deployment region

$$S_{E_{4_e}}(r, x, y) = L^2 \tag{12}$$

The functions for the various regions presented above are independent of each other and therefore,  $\mu(r)$  can be calculated separately for each region and summed together for the final result.

$$\mu(r) = \mu_A(r) + \mu_B(r) + \mu_C(r) + \mu_D(r) + \mu_E(r)$$

Figure 12 demonstrates the boundary effect by representing the recently described  $S(r, x, y)$  as the number of neighboring mobile nodes within the transmission range of a node moving away from a corner of the map (Region  $C$ ). The  $x$  and  $y$  axes of the figure represent the node's location in one quarter of a deployment map and the  $z$  axis shows the number of nodes in a given transmission range. The figure shows that as the node moves away from a corner or a map edge, the number of nodes connected directly to the node increases until it reaches a constant.

#### IV. RANDOM WALK ANALYTICAL MODEL

In the previous chapter, Equation 1 was introduced as a model for effective connectivity. This section outlines the adaptation of the effective connectivity model for use with the random walk mobility model. Section II outlined the regional differences for calculating  $S(r, x, y)$ . These functions for  $S(r, x, y)$  along with the probability  $p(x, y)$  of a node's location under the random walk mobility model will be used in this adaptation.

MNs under the random walk mobility model remain distributed uniformly during the entire simulation [5], [13]. Therefore, the function  $p(x, y)$  associated with Equation 1 can be found by once again referring to Figures 2(a) and 2(b). The probability that a node is located at a given  $(x, y)$  is identical for every point within a region. This function is derived from the uniform density of the random walk mobility model. Therefore, it is equivalent to the ratio of the area of a region to the area of the entire deployed region. When  $r \leq \frac{L}{2}$  the probabilities are as follows:

$$p_A(x, y) = \left(1 - 2\frac{r}{L}\right)^2 \quad (13)$$

$$p_B(x, y) = 4\left(1 - 2\frac{r}{L}\right)\frac{r}{L} \quad (14)$$

$$p_C(x, y) = 4\left(\frac{r}{L}\right)^2 \quad (15)$$

When  $\frac{L}{2} < r \leq L$  the probabilities are:

$$p_C(x, y) = 4 \cdot \left(1 - \frac{r}{L}\right)^2 \quad (16)$$

$$p_D(x, y) = -4 \cdot \left(2\frac{r}{L} - 1\right) \cdot \left(\frac{r}{L} - 1\right) \quad (17)$$

$$p_E(x, y) = \left(2\frac{r}{L} - 1\right)^2 \quad (18)$$

These probabilities are then used along with the functions,  $S(r, x, y)$ , for coverage area given in the Section II and inserted into Equation 1 to determine the effective connectivity.  $\mu(r)$  is divided into separate calculations for each region and summed together at the end for the resulting random walk effective connectivity model.

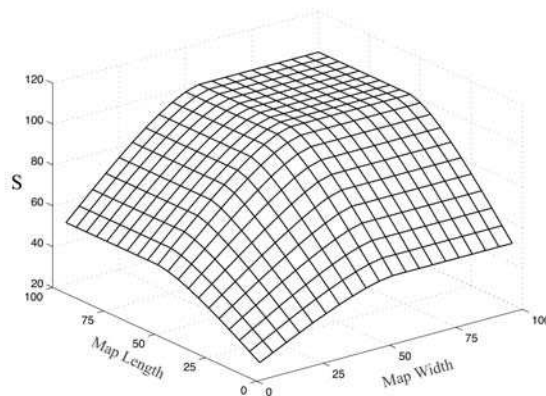


Fig. 12. Effective Transmission area due to border effect

### A. Region A

For Region A, Equations 2 and 13 are brought together with 1 to form the following completed equation

$$\mu_A(r) = \pi r^2 \cdot \left(1 - 2\frac{r}{L}\right)^2 \quad (19)$$

### B. Region B

Because Equation 3 for Region B is dependent on  $x$ , when this equation and Equation 14 are inserted into Equation 1,  $\mu_B$  must be integrated with respect to  $x$  over 0 to  $r$  to determine an equation for effective connectivity based on  $r$ . Integrating this region results in a volume and therefore, must include a division by  $r$ , the length of  $x$ , to return this function to an area. When the integration is performed on

$$\mu_B(r) = \int_r^{L-r} \int_0^r \frac{S_B(r, x, y) \cdot p_B(x, y) dx, dy}{r}$$

the resulting equation for Region B is

$$\mu_B(r) = \frac{4r^3(3\pi - 2)(L - 2r)}{3L^2} \quad (20)$$

### C. Region C

Region C for  $r \leq \frac{L}{2}$  was previously divided into two separate cases. These two sub-cases, Case  $C_1$  and Case  $C_2$ , contained within C both utilize the same probability shown in Equation 15 but have different equations. Because these functions are integrated with respect to both  $x$  and  $y$ , the final product of  $\mu_C$  must be divided by the area of Region C,  $r^2$ , so that  $\mu_C$  represents an effective area. The resulting equations for Region C when  $r \leq \frac{L}{2}$  are

Case  $C_1$

$$\mu_{C_3}(r) = \frac{\int_0^{\sqrt{r^2-x^2}} \int_0^r S_{C_3}(r, x, y) \cdot p_C(x, y) dy dx}{r^2}$$

Case  $C_2$

$$\mu_{C_3}(r) = \frac{\int_{\sqrt{r^2-x^2}}^r \int_0^r S_{C_3}(r, x, y) \cdot p_C(x, y) dy dx}{r^2}$$

upon integration and summation of  $\mu_{C_3}(r)$  from Case  $C_1$  and Case  $C_2$  the resulting equation for Region C when  $r \leq \frac{L}{2}$  is

$$\mu_C(r) = \frac{r^4(13\pi - 10)}{4L^2} \quad (21)$$

When  $\frac{L}{2} < r \leq L$ , the final function must still be divided by the area of Region C so that it represents an effective area, however this area has changed and is now  $(L - r)^2$ . The probability for this sub-case is shown in Equation 16. As was mentioned in Section II, Region C for  $\frac{L}{2} < r \leq L$  is only based on the first case of C. The resulting equation for Region C when  $\frac{L}{2} < r \leq L$  is

$$\mu_{C_3}(r) = \frac{\int_0^{L-r} \int_0^{L-r} S_{C_3}(r, x, y) \cdot p_C(x, y) dx dy}{(L - r)^2}$$

and after integrating, Region  $C$  for  $\frac{L}{2} < r \leq L$  is represented as

$$\begin{aligned} \mu_{C_3}(r) = & \frac{L-r}{3L^2} \left[ 3L^3 + 4L^2 \sqrt{-L(L-2r)} - 9rL^2 - 3Lr^2\pi - 8L\sqrt{-L(L-2r)}r \right. \\ & + 9\pi r^2L - 6r^2 \arccos\left(\frac{L-r}{r}\right)L + 9r^2L + 6Lr^2 \arcsin\left(\frac{L-r}{r}\right) \\ & - 11r^3 - 9\pi r^3 + 3r^3\pi + 12r^2 \sqrt{-L(L-2r)} - 6r^3 \arcsin\left(\frac{L-r}{r}\right) \\ & \left. + 6r^3 \arccos\left(\frac{L-r}{r}\right) \right] \end{aligned} \quad (22)$$

#### D. Region $D$

The portion of the random walk effective connectivity formula related to Region  $D$  comes from Equations 6 and 17. Once again the area that the region covers will be included in the denominator so that the final function results in the effective area of Region  $D$ . The area of Region  $D$  is  $(2r-L)(L-r)$ . After combining the area and the two equations mentioned above with Equation 1 the resulting function is

$$\mu_D(r) = \frac{\int_{L-r}^r \int_0^{L-r} S_D(r, x, y) \cdot p_D(x, y) dx dy}{(2r-L)(L-r)}$$

and Region  $D$  after integration is

$$\begin{aligned} \mu_D(r) = & \frac{-2(L-r)}{3L^2} \left[ 3L^3 - 9L^2r + 6Lr^2 \arcsin\left(\frac{L-r}{r}\right) + 6Lr^2 + 3r^2\pi L \right. \\ & - 3r^2\pi L - 2(-L(L-2r))^{3/2} + 6r^2 \sqrt{-L(L-2r)} \\ & \left. + 3r^3\pi - 6r^3 \arcsin\left(\frac{L-r}{r}\right) - 6r^3\pi \right] \end{aligned} \quad (23)$$

#### E. Region $E$

The portion of the effective connectivity formula for Region  $E$  is made up of Region  $E$ 's sub-cases as detailed in Section II. The calculation of  $\mu_E(r)$  is highly dependent on  $r$  and each sub-case is only used in the final equation for a specific range of  $r$ .

As done for the previous regions, these functions must be multiplied by the probability from Equation 18 and divided by the area of Region  $E$ ,  $(2r-L)^2$ . These two factors are constants in the integration as they are completely independent of  $(x, y)$ .

1) *Sub-case  $E_1$* :: The range for this region was defined as  $\frac{L}{2} < r \leq (2-\sqrt{2})L$  in Section II and it was also explained that there was only one formula for this sub-case. The function for  $\mu$  in this first sub-case is

$$\mu_{E_1}(r) = \frac{\int_{L-r}^r \int_{L-r}^r S_{E_1}(r, x, y) \cdot p_E(x, y) dx dy}{(2r-L)^2}$$

after integration, Region  $E$  for  $\frac{L}{2} < r \leq (2-\sqrt{2})L$  is

$$\begin{aligned} \mu_{E_1}(r) = & \frac{-r^2}{L^2} (2r-L) \left[ 4r \arcsin\left(\frac{-L+r}{r}\right) \right. \\ & \left. - 4L \arcsin\left(\frac{-L+r}{r}\right) - L\pi + 4\sqrt{L(2r-L)} \right] \end{aligned} \quad (24)$$

2) *Sub-case  $E_2$* :: From Section II it is known that sub-case  $E_2$  involves two sub-regions,  $E_{2a}$  and  $E_{2b}$ , that sum together to form the equation for sub-case  $E_2$ . To simplify the calculations, Region  $E$  was divided into 4 symmetric quadrants. The limits of integration for  $E_{2a}$  and  $E_{2b}$  are derived from Figure 9(a). Each of the functions includes a factor of 4 to allow for all four symmetric quadrants. The resulting equations for Region  $E$  when  $(2 - \sqrt{2})L < r \leq \frac{5}{8}L$  are:

$$\mu_{E_{2a}}(r) = \frac{4 \cdot p_E(x, y)}{(2r - L)^2} \cdot \left[ \int_{L-r}^{\frac{L}{2}} \int_{\sqrt{2Lr-L^2}}^{\frac{L}{2}} S_{E_{2a1}} dx dy \right. \\ \left. + \int_{L-r}^{\sqrt{2Lr-L^2}} \int_{-x+L-r+\sqrt{2Lr-L^2}}^{\frac{L}{2}} S_{E_{2a2}} dy dx \right]$$

$$\mu_{E_{2b}}(r) = \frac{4 \cdot p_E(x, y)}{(2r - L)^2} \cdot \int_{L-r}^{-x+L-r+\sqrt{2Lr-L^2}} \int_{L-r}^{\sqrt{2Lr-L^2}} S_{E_{2b}} dy dx$$

that upon integration result in the following two equations to be used when  $(2 - \sqrt{2})L < r \leq \frac{5}{8}L$ .

$$\begin{aligned} \mu_{E_{2a}}(r) = & \frac{r^2}{L^2} \left[ r^2 \pi - 2r^2 \arcsin \left( \frac{\sqrt{2Lr-L^2}}{r} \right) - 2r^2 \arcsin \left( \frac{-\sqrt{2Lr-L^2}+L}{r} \right) \right. \\ & + 8\sqrt{2Lr-L^2} \arcsin \left( \frac{-\sqrt{2Lr-L^2}+L}{r} \right) L - 6r\sqrt{-L(-2r+L)} \\ & - 6\sqrt{r^2+2\sqrt{2Lr-L^2}L-2LrL} + 6r^2 \arcsin \left( \frac{-r+L}{r} \right) + 2rL\pi \\ & + 2\sqrt{-L(-2r+L)}L + 4 \arcsin \left( \frac{\sqrt{2Lr-L^2}}{r} \right) L^2 \\ & - 4rL \arcsin \left( \frac{-r+L}{r} \right) - 8r\sqrt{2Lr-L^2} \arcsin \left( \frac{-r+L}{r} \right) \\ & - 8 \arcsin \left( \frac{\sqrt{2Lr-L^2}}{r} \right) Lr - 8 \arcsin \left( \frac{-\sqrt{2Lr-L^2}+L}{r} \right) Lr \\ & - 6\sqrt{r^2-2Lr+L^2}\sqrt{2Lr-L^2} + 4\pi Lr - L^2\pi - 4\sqrt{2Lr-L^2}L\pi \\ & + 8\sqrt{2Lr-L^2}L \arcsin \left( \frac{-r+L}{r} \right) + 8\sqrt{2Lr-L^2}\sqrt{-L(-2r+L)} \\ & \left. + 6\sqrt{r^2+2\sqrt{2Lr-L^2}L-2Lr}\sqrt{2Lr-L^2} \right] \end{aligned} \quad (25)$$

$$\begin{aligned}
\mu_{E_2b}(r) = & \frac{-1}{6L^2} \left[ -24r^3 \arcsin\left(\frac{t - \sqrt{t}\sqrt{-t+2r}}{r}\right) t - 24r^3 \arcsin\left(\frac{-t+r}{r}\right) t \right. \\
& + 12r^2 \arcsin\left(\frac{-t+r}{r}\right) t^2 + 9r^4 \arcsin\left(\frac{-t+r}{r}\right) - 10t^{3/2}r^2\sqrt{-t+2r} \\
& - 12t^{5/2}\sqrt{-t+2r}r + 18r^3\sqrt{t}\sqrt{-t+2r} - 120t^2r^2 + 80t^3r - 20t^4 \\
& + 8t^{5/2}\sqrt{r^2 - 2tr + 2t^{3/2}\sqrt{-t+2r}\sqrt{-t+2r}} - 6r^3\pi\sqrt{t}\sqrt{-t+2r} \\
& + 8t^3\sqrt{r^2 - 2tr + 2t^{3/2}\sqrt{-t+2r}} - 24r^3t \arcsin\left(\frac{\sqrt{t}\sqrt{-t+2r}}{r}\right) \\
& + 24r^3 \arcsin\left(\frac{-t+r}{r}\right) \sqrt{t}\sqrt{-t+2r} + 24r^3t \arcsin\left(\frac{-t + \sqrt{t}\sqrt{-t+2r}}{r}\right) \\
& + 8t^{3/2}r\sqrt{r^2 - 2tr + 2t^{3/2}\sqrt{-t+2r}\sqrt{-t+2r}} + 4t^{7/2}\sqrt{-t+2r} \\
& - 24r^2t^{3/2} \arcsin\left(\frac{-t+r}{r}\right) \sqrt{-t+2r} + 12r^2t^2 \arcsin\left(\frac{\sqrt{t}\sqrt{-t+2r}}{r}\right) \\
& + 26r^2\sqrt{r^2 - 2tr + 2t^{3/2}\sqrt{-t+2r}\sqrt{t}\sqrt{-t+2r}} - 18r^2\pi t^{3/2}\sqrt{-t+2r} \\
& - 24r^2t^{3/2}\sqrt{-t+2r} \arcsin\left(\frac{-t + \sqrt{t}\sqrt{-t+2r}}{r}\right) + 24r^3\pi t + 80tr^3 \\
& - 24t^2\sqrt{r^2 - 2tr + 2t^{3/2}\sqrt{-t+2r}r} - 6r^4 \arcsin\left(\frac{t - \sqrt{t}\sqrt{-t+2r}}{r}\right) \\
& - 26r^2\sqrt{r^2 - 2tr + 2t^{3/2}\sqrt{-t+2r}} - 3r^4 \arcsin\left(\frac{\sqrt{t}\sqrt{-t+2r}}{r}\right) \\
& \left. + 24r^2 \arcsin\left(\frac{t - \sqrt{t}\sqrt{-t+2r}}{r}\right) t^{3/2}\sqrt{-t+2r} - 5r^4 \right] \quad (26)
\end{aligned}$$

These two equations show how rapidly the complicated sub-cases of Region  $E$  grow into vastly complicated formulas for the effective coverage of the random walk mobility model. The following two sub-cases,  $E_3$  and  $E_4$ , quickly become even more complex and for this reason the result of their integrations will not fit on these pages.

3) *Sub-case  $E_3$* :: For  $\frac{5}{8}L < r \leq \frac{L}{\sqrt{2}}$  sub-case  $E_3$  becomes the function for Region  $E$ . This sub-case was previously defined in Section II and is made up of three separate sub-regions. As with the previous sub-cases, the equations for  $S_{E_3}$  must be inserted into the equation for  $\mu$  and integrated. Choosing limits of integration becomes rather complicated in this sub-case. Figure 13 represents the lower left quarter of Region  $E$  for this sub-case. This figure is used to determine the limits of integration. The dashed lines in this figure are the arcs located a distance of  $r$  from the corners of the deployment as explained in Section II. These lines are curved, but are estimated as straight lines for the purpose of simplifying the integrations. This can be done with minimal error. From this figure, the functions for these dashed lines are

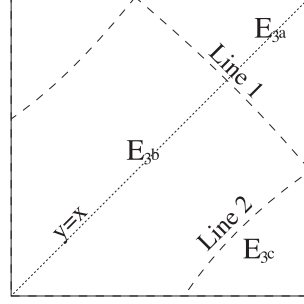
*Line<sub>1</sub>*

$$y(x) = \sqrt{2tr - t^2} + \left[ \frac{\sqrt{2tr - t^2} - t + r}{t - r - \sqrt{2tr - t^2}} \right] (x - t + r)$$

*Line<sub>2</sub>*

$$\begin{aligned}
y(x) = & \frac{-1}{4 \left( -t + tr - \sqrt{-(-2r+t)tr} \right)} [2xr\sqrt{4r^2 - t^2} - 4xtr + 4xr^2 \\
& + 2\sqrt{4r^2 - t^2}t - 3\sqrt{4r^2 - t^2}tr + 2\sqrt{4r^2 - t^2}\sqrt{-(-2r+t)tr} + 2rt^2 - 2tr^2]
\end{aligned}$$

Using the figure and the above formulas for the lines in the figure the equations for Region  $E$  when

Fig. 13. Sub-case  $E_3$ 

$\frac{5}{8}L < r \leq \frac{L}{\sqrt{2}}$  are

$$\mu_{E_{3a}}(r) = \frac{4 \cdot p_E(x, y)}{(2r - L)^2} \cdot \int_{\sqrt{r^2 - \frac{L^2}{4}}}^{\frac{L}{2}} \int_{\sqrt{r^2 - x^2}}^{\frac{L}{2}} S_{E_{3a}} dx dy$$

$$\mu_{E_{3b}}(r) = \frac{p_E(x, y)}{(2r - L)^2} \cdot \left[ 8 \cdot \int_{L-r}^{\frac{L}{2}} \int_{L-r}^x S_{E_{3b}} dy dx \right. \\ \left. - 4 \cdot \int_{\sqrt{r^2 - \frac{L^2}{4}}}^{\frac{L}{2}} \int_{line_1}^{\frac{L}{2}} S_{E_{3b}} dy dx - 8 \cdot \int_{-(\sqrt{r^2 - (L-r)^2} - L)}^{\frac{L}{2}} \int_{L-r}^{Line_2} S_{E_{3b}} dy dx \right]$$

$$\mu_{E_{3c}}(r) = \frac{8 \cdot p_E(x, y)}{(2r - L)^2} \cdot \int_{-(\sqrt{r^2 - (L-r)^2} - L)}^{\frac{L}{2}} \int_{L-r}^{Line_2} S_{E_{3c}} dy dx$$

The above multipliers of either 4 or 8 are inserted into the function based on the symmetric regions. Once again referring to Figure 13 it can be seen that the equation for sub-region  $E_{3a}$  is integrated over a quarter of the subregion and therefore, this equation must be multiplied by 4 to include the entire sub-region. Sub-regions  $E_{3b}$  and  $E_{3c}$  shown in this figure are integrated over just  $\frac{1}{8}$  of their entire area and are therefore multiplied by 8. Sub-region  $E_{3b}$  was calculated by integrating it over the entire area under the line  $y = x$  and then subtracting out the portions outside of  $E_{3b}$ . This proved to be the most efficient way to calculate this sub-region.

4) *Sub-case  $E_4$* : The final sub-case for Region  $E$  is for  $\frac{L}{\sqrt{2}} < r \leq L$  and is made up of four sub-regions. These sub-regions were defined in Section II and shown in Figure 7(d). As with sub-case  $E_3$ , choosing the limits of integration for this sub-case proved to be a challenge. Figure 14 shows the breakup of the sub-regions for this sub-case. As was the case in the previous figures, this figure is the lower left quarter of Region  $E$ . The dashed lines are the arcs located a distance of  $r$  from the corners of the deployment. The two dotted lines are displayed for reference. From this figure, the functions for these dashed lines are

*Line<sub>3</sub>*

$$y(x) = \frac{1}{L - \sqrt{-L^2 + 4r^2}} L^2 - 2\sqrt{-L^2 + 4r^2}L - Lx + \sqrt{-L^2 + 4r^2}x + 2r^2$$

*Line<sub>4</sub>*

$$y(x) = L - \sqrt{r^2 - x^2}$$

*Line<sub>5</sub>*

$$y(x) = L - r + \left[ \frac{\frac{L}{2} - r + \frac{1}{2}\sqrt{2r^2 - L^2}}{\frac{1}{2}L - \sqrt{2}Lr - L^2 + \frac{1}{2}\sqrt{2r^2 - L^2}} \right] (x - t + \sqrt{2}Lr - L^2)$$

As shown in the figure,  $E_{4c}$  is further divided into two zones,  $E_{4c_1}$  and  $E_{4c_2}$  for ease of computation. As occurred in the previous sub-case, sub-region  $E_{4b}$  will be integrated under the line  $y = x$  from the corner,  $(L - r)$ , to the dotted line dividing the sub-region  $E_{4c}$  in two. This will be followed by subtracting the function  $S_{E_{4b}}$  integrated over the bounds of sub-region  $E_{4c_2}$ . This was found to be the least complicated method. The integration of sub-region  $E_{4d}$  is performed similar to that of  $E_{4b}$ . With the use of these considerations the functions for Region  $E$  for sub-case  $E_4$  are

$$\begin{aligned} \mu_{E_{4b}}(r) &= \frac{8 \cdot p_E(x, y)}{(2r - L)^2} \cdot \left[ \int_{L-r}^{\frac{L}{2} - \frac{1}{2}\sqrt{2r^2 - L^2}} \int_{L-r}^x S_{E_{4b}} dy dx \right. \\ &\quad \left. - \int_{L - \sqrt{2Lr - L^2}}^{\frac{L}{2} - \frac{1}{2}\sqrt{2r^2 - L^2}} \int_{L-r}^{Line_5} S_{E_{4b}} dy dx \right] \\ \mu_{E_{4c_1}}(r) &= \frac{8 \cdot p_E(x, y)}{(2r - L)^2} \cdot \int_{\frac{L}{2} - \frac{1}{2}\sqrt{2r^2 - L^2}}^{\frac{L}{2}} \int_{L-r}^{Line_4} S_{E_{4c}} dy dx \\ \mu_{E_{4c_2}}(r) &= \frac{8 \cdot p_E(x, y)}{(2r - L)^2} \cdot \int_{L - \sqrt{2Lr - L^2}}^{\frac{L}{2} - \frac{1}{2}\sqrt{2r^2 - L^2}} \int_{L-r}^{Line_5} S_{E_{4c}} dy dx \\ \mu_{E_{4d}}(r) &= \frac{p_E(x, y)}{(2r - L)^2} \cdot \left[ 8 \cdot \int_{\frac{L}{2} - \frac{1}{2}\sqrt{2r^2 - L^2}}^{\frac{L}{2}} \int_{L-r}^x S_{E_{4d}} dy dx \right. \\ &\quad \left. - 4 \cdot \int_{L - \sqrt{r^2 - \frac{L^2}{4}}}^{\frac{L}{2}} \int_{Line_3}^{\frac{L}{2}} S_{E_{4d}} dy dx - 8 \cdot \int_{\frac{L}{2} - \frac{1}{2}\sqrt{2r^2 - L^2}}^{\frac{L}{2}} \int_{L-r}^{Line_4} S_{E_{4d}} dy dx \right] \\ \mu_{E_{4e}}(r) &= \frac{4 \cdot p_E(x, y)}{(2r - L)^2} \cdot \int_{L - \sqrt{r^2 - \frac{L^2}{4}}}^{\frac{L}{2}} \int_{Line_3}^{\frac{L}{2}} S_{E_{4e}} dy dx \end{aligned}$$

After performing all the necessary calculations for the effective connectivity of the random waypoint mobility model, we are left with the following complex formula

$$\mu(r) = \begin{cases} \mu_A(r) + \mu_B(r) + \mu_C(r) & \text{if } 0 < r \leq \frac{L}{2} \\ \mu_{C_3}(r) + \mu_D(r) + \mu_{E_1}(r) & \text{if } \frac{L}{2} < r \leq (2 - \sqrt{2})L \\ \mu_{C_3}(r) + \mu_D(r) + \mu_{E_{2a}}(r) + \mu_{E_{2b}}(r) & \text{if } (2 - \sqrt{2})L < r \leq \frac{5L}{8} \\ \mu_{C_3}(r) + \mu_D(r) + \mu_{E_{3a}}(r) + \mu_{E_{3b}}(r) + \mu_{E_{3c}}(r) & \text{if } \frac{5L}{8} < r \leq \frac{L}{\sqrt{2}} \\ \mu_{C_3}(r) + \mu_D(r) + \mu_{E_{4b}}(r) + \mu_{E_{4c-1}}(r) \\ \quad + \mu_{E_{4c_2}}(r) + \mu_{E_{4d}}(r) + \mu_{E_{4e}}(r) & \text{if } \frac{L}{\sqrt{2}} < r \leq L \end{cases}$$

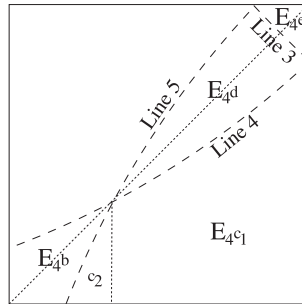


Fig. 14. Sub-case  $E_4$

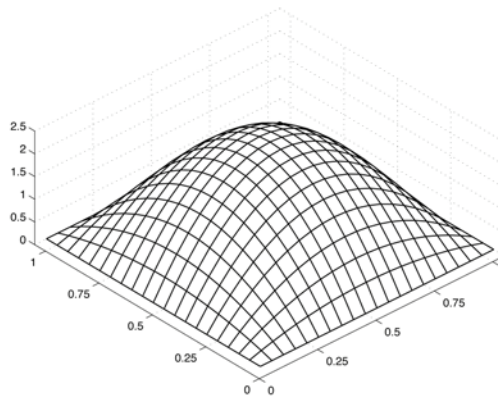


Fig. 15. Spatial Distribution of Random Waypoint

It has been found that this model can be simplified to just the first three regions and expanded over the entire range of  $r$  instead of limiting them to  $r \leq \frac{L}{2}$ . This drastically simplifies the model. The resulting equation for effective connectivity in the random walk mobility model is

$$\mu(r) = \frac{\pi r^2(L - 2r)^2}{L^2} + \frac{4r^3(3\pi - 2)(L - 2r)}{3L^2} + \frac{r^4(9\pi - 5)}{3L^2} \quad (27)$$

This much shorter and simpler version of  $\mu(r)$  is compared with the longer version and analyzed for accuracy in Chapter 6.

Equation 27 can be converted into a relative mean effective connectivity model by dividing it by the deployed area,  $L^2$ , so that it becomes unit-less. The substitution

$$\rho = \frac{r}{L}$$

can be made so that Equation 27 becomes a function of the transmission range and the deployment area

$$\mu(\rho) = \left(\frac{11}{3} - \pi\right)\rho^4 - \frac{8}{3}\rho^3 + \pi\rho^2 \quad (28)$$

The resulting relative mean effective connectivity function, Equation (28), can be plotted over a range of transmission ranges to give us a visual representation of how node connectivity will be effected as transmission range is increased.

## V. RANDOM WAYPOINT ANALYTICAL MODEL

In a similar manner to the previous section regarding random walk, this section will outline the adaptation of the effective connectivity model for use with the random waypoint mobility model. The functions outlined in Chapter 3 for calculating  $S(r, x, y)$  will again be used in this implementation along with the probability  $p(x, y)$  of a node's location under the random waypoint mobility model.

The random waypoint mobility model lacks the uniform distribution of the random walk model. Because of this, the spatial node density must be taken into consideration. Many researchers have worked to derive functions for the random waypoint spatial density [2], [4], [12], [13]. This research uses the simplified function presented in [13] for this adaptation of the effective connectivity model to the random waypoint model. Figure 15 represents the resulting distribution of the random waypoint model using [13].

The effective connectivity of nodes within these regions is calculated similar for this model as it was for the random walk model, with the inclusion of the spatial node density function from [13]. Due to this inclusion,  $S(r, x, y)$  becomes not only a function of area, but also a function of density.

$$S(r, x, y) = f(A(r, x, y), p(x, y)) \quad (29)$$

Computing the probabilities for this model involve the use of the spatial density function from [13] discussed earlier. To simplify the calculations a zero pause time is assumed and no node is stationary at the beginning of the simulation. The resulting simplified spatial density function is,

$$f(x, y) = 36xy(x-1)(y-1) \quad (30)$$

and is based on a unit square map. The actual probability that a node is located at a given  $(x, y)$  becomes a function of the area under Equation (30). This will result in an equation for effective connectivity in the random waypoint mobility model that is based on the unit square. The resulting function is similar to that for random walk, that is, it is a function of transmission range versus deployment area.

Again,  $\mu(r)$  is calculated separately for each of the regions and combined in the end for the final result. Due to the accuracy of the simplified random walk model and the complexity of the full version of the random walk analytical model, only the simplified version of the random waypoint analytical model has been calculated.

### A. Region A

Region A again comes from Figure 2(a) and is calculated by combining the Equations 2, 29 and 30. The new combined equation is a function of both  $x$  and  $y$  and is therefore integrated over  $r$  to  $L-r$  for both  $x$  and  $y$ . The equation for Region A is

$$\mu_A(r) = \int_r^{L-r} \int_r^{L-r} S_A(r, x, y) \cdot [36xy(x-L)(y-L)]^2 dx dy$$

which upon integration the equation becomes

$$\begin{aligned} \mu_A(r) = & \frac{36}{25} r^2 \pi - \frac{288}{5} \pi r^5 + \frac{432}{5} r^6 \pi - \frac{864}{25} \pi r^7 + 576 \pi r^8 \\ & - 1728 r^9 \pi + \frac{9936}{5} r^{10} \pi - \frac{5184}{5} r^{11} \pi + \frac{5184}{25} r^{12} \pi \end{aligned} \quad (31)$$

### B. Region B

Again Region B is symmetric and therefore one needs only to derive a calculation for one of the B regions. As was the case in the calculation for Region B under the random walk analytical model, using region  $B_1$  from Figure 2(a). In this analytical equation Region B is dependent on both the  $x$  and  $y$  variables and must be integrated over both. It can be seen in Figure 2(a) that Region B is to be integrated with respect to  $x$  over 0 to  $r$  and with respect to  $y$  over  $r$  to  $L-r$ . By combining Equations 3, 29 and 30, Region B is

$$\mu_B(r) = 4 \cdot \int_r^{L-r} \int_0^r S_B(r, x, y) \cdot [36xy(x-L)(y-L)]^2 dx dy$$

the resulting equation becomes

$$\begin{aligned} \mu_B(r) = & \left( \frac{288}{5} \pi - \frac{384}{25} \right) r^5 - \frac{405}{5} \pi r^6 + \left( \frac{864}{25} \pi - \frac{4608}{875} \right) r^7 \\ & + \left( \frac{1536}{5} - 1152 \pi \right) r^8 + \left( 3348 \pi - \frac{2304}{5} \right) r^9 + \left( \frac{50688}{175} - \frac{19062}{5} \pi \right) r^{10} \\ & + \left( \frac{10044}{5} \pi - \frac{27648}{175} \right) r^{11} + \left( \frac{55296}{875} - \frac{10368}{25} \pi \right) r^{12} \end{aligned} \quad (32)$$

### C. Region C

As with the previous derivation of the random walk analytical model, Region  $C$  of this model is not only symmetric but also broken into the same two sub-cases,  $C_1$  and  $C_2$ . Both of these functions use the same limits of integration as was used for the random walk analytical model, however they are now combined with Equations 29 and 30 to form

Case  $C_1$

$$\mu_{C_1}(r) = \int_0^{\sqrt{r^2-x^2}} \int_0^r S_{C_3}(r, x, y) \cdot [36xy(x-L)(y-L)]^2 dx dy$$

Case  $C_2$

$$\mu_{C_2}(r) = \int_{\sqrt{r^2-x^2}}^r \int_0^r S_{C_3}(r, x, y) \cdot [36xy(x-L)(y-L)]^2 dy dx$$

after integrating and combining the two formulas, the equation for Region  $C$  is

$$\begin{aligned} \mu_C(r) = & \left( \frac{9531}{20} \pi + \frac{1578}{175} \right) r^8 + \left( \frac{93984}{1225} - \frac{60048}{35} \pi \right) r^9 \\ & + \left( \frac{431649}{224} \pi - \frac{742248}{1225} \right) r^{10} + \left( \frac{6258496}{13475} - \frac{74889}{10} \pi \right) r^{11} \\ & + \left( \frac{10886404}{67375} + \frac{760707}{5600} \pi \right) r^{12} \end{aligned} \quad (33)$$

Now that all the required calculations have been performed for the random walk analytical model, the individual regional functions are combined to form the full model.

$$\begin{aligned} \mu(r) = & \frac{36}{25} \pi r^2 - \frac{384}{25} r^5 + \frac{27}{5} \pi r^6 - \frac{4608}{875} r^7 \\ & + \left( \frac{55338}{175} - \frac{1989}{20} \pi \right) r^8 + \left( -\frac{470496}{1225} + \frac{4212}{35} \pi \right) r^9 \\ & + \left( -\frac{387432}{1225} + \frac{114021}{1120} \pi \right) r^{10} + \left( \frac{165184}{539} - \frac{6849}{70} \pi \right) r^{11} \\ & + \left( \frac{15144196}{67375} - \frac{400509}{5600} \pi \right) r^{12} \end{aligned} \quad (34)$$

Because this function is based on the unit square, the transmission range,  $r$ , in this model is already the ratio of transmission range to map length,  $\frac{r}{L}$ . Therefore,  $r$  can be substituted with  $\rho$  in Equation 34 to match the random walk analytical model.

$$\begin{aligned} \mu(\rho) = & \frac{36}{25} \pi \rho^2 - \frac{384}{25} \rho^5 + \frac{27}{5} \pi \rho^6 - \frac{4608}{875} \rho^7 \\ & + \left( \frac{55338}{175} - \frac{1989}{20} \pi \right) \rho^8 + \left( -\frac{470496}{1225} + \frac{4212}{35} \pi \right) \rho^9 \\ & + \left( -\frac{387432}{1225} + \frac{114021}{1120} \pi \right) \rho^{10} + \left( \frac{165184}{539} - \frac{6849}{70} \pi \right) \rho^{11} \\ & + \left( \frac{15144196}{67375} - \frac{400509}{5600} \pi \right) \rho^{12} \end{aligned} \quad (35)$$

Both this model and the random walk analytical model will be analyzed and compared to simulated data in the next section.

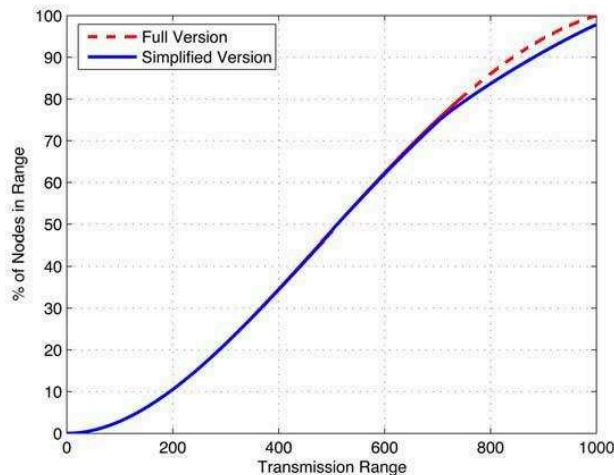


Fig. 16. Complete and Simplified

## VI. ANALYSIS

### A. Random Walk Analytical vs Simulated

Section IV presented two versions of the random walk analytical model. The first version is a complete implementation of the effective coverage analytical model over the range of  $0 < r \leq L$  made up of several parts. The second version is an expansion of the simpler beginning part of the lengthy first version. This function was originally intended to represent the effective coverage of the random walk mobility model from  $0 < r \leq \frac{L}{2}$ . However, once it was implemented the range was experimented with and it was found that its output is nearly identical to that of the lengthier version all the way to the extreme end of the range,  $L$ . Figure 16 shows both of these equations plotted together on the same graph. As one can see from the figure, the two functions are nearly identical all the way to about  $r = 750$ . At this point the simplified version produces a slightly lower estimation than the full version. Figure 17 shows both of these versions plotted with the results of a simulation. In this figure, it is clear that both models slightly deviate from the simulated data with the full version slightly over estimating and the abbreviated version slightly under estimating. The differences at this level of  $r$  are negligible as these levels of transmission range versus deployment region are not realistic. Therefore, the simplified version provides functional results.

To compare the model with the simulated data, multiple random walk simulations were run with the total number of simulated nodes ranging from 20 to 300 in increments of 20. Each of these simulations was conducted with a map size of  $1000 \times 1000$  meters, a simulation time of 900 seconds, minimum node speed of 0.1 meters/second, maximum node speed of 10 meters/second and a uniformly distributed duration of  $[0, 100]$  seconds. Data from every simulation was then analyzed, at transmission ranges from 25 meters to 1000 meters, for the average number of nodes within one node's transmission range. The data was plotted as the average percentage of nodes in the simulation that are within the transmission range of one node. As the transmission range increased, the curves of all simulations followed the same shape regardless of the number of nodes in the simulation.

The random walk simulation data was plotted with the random walk analytical model and can be seen by once again referring to Figure 17. From this figure one can see that the random walk simulation data and the random walk analytical model are nearly identical. The most noticeable difference in the analytical model as compared to the simulation data occurs at the upper bounds of the transmission range. This is attributed mainly to the approximation used in the analytical model. The analytical model is accurate up to approximately  $r = \frac{3L}{4}$ , this is where the simplified model deviates from the full model and the curve is slightly skewed.

The fourth curve in Figure 17 represents the behavior of node coverage if no cutoff is taken into

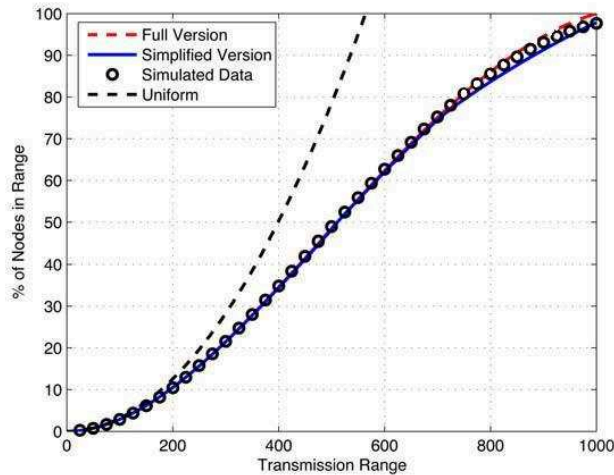


Fig. 17. Complete, Simplified and Simulated

consideration, that is, a uniform coverage area is assumed. For a relatively small transmission range this assumption could be acceptable, but as the transmission range increases the assumed and actual node coverage differ greatly.

The analytical model and the uniform model are compared with the random walk simulation data and the difference is plotted in Figure 18. From this figure, it can be seen that the level of error increases at an exponential rate for the uniform distribution as  $r$  is increased. However, the analytical model retains a very small level of error throughout all values of  $r$ . From this data, it can be concluded that the uniform distribution can be used with a 95% confidence level if  $r \leq 75$  and with a 90% confidence level if  $r \leq 125$ . These confidence levels decrease at a rapid rate beyond  $r = 125$ . However, using the analytical model the confidence level never drops below 95% and is actually better than 97.5% for  $r \leq 900$ .

### B. Random Waypoint Analytical vs Simulated

As with the random walk simulations, multiple simulations were run for the random waypoint model. The number of nodes, simulation map size and simulation time was the same as in the random walk simulations. However, duplicate simulations were run with different speed ranges. The first simulation set was run with a minimum and maximum speed identical to that of the random walk simulations. The second simulation set was configured with a minimum and maximum speed of 5 meters/second. The maximum rest time for a node in both simulation sets was set to zero. Again data from each simulation was analyzed, at transmission ranges from 25 meters to 1000 meters, for the average number of nodes

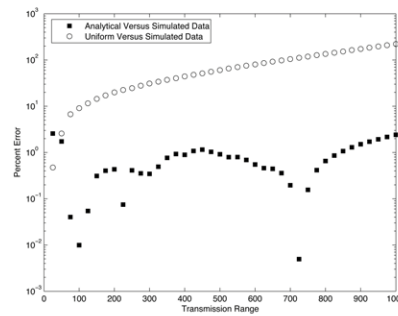


Fig. 18. Error of Random Walk

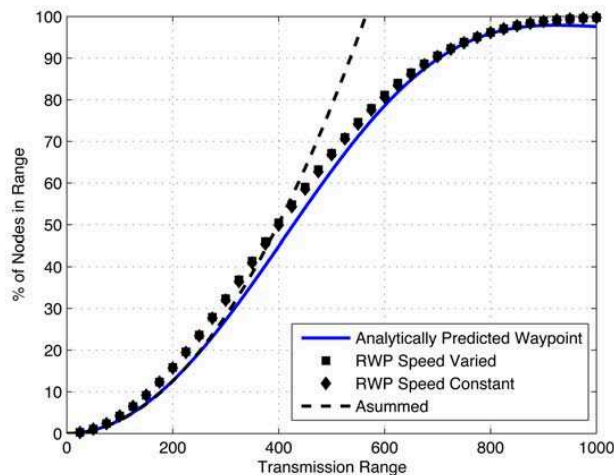
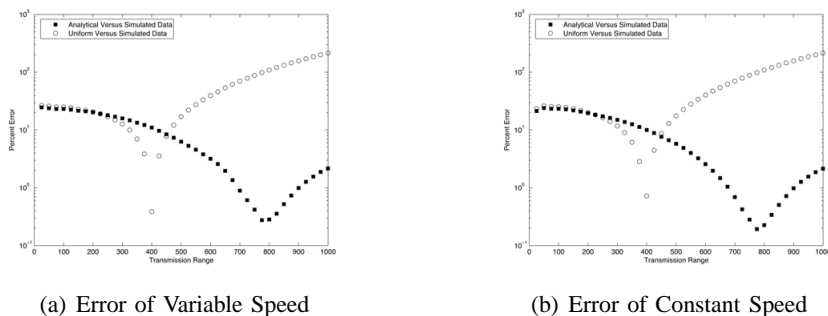


Fig. 19. Comparison of Random Waypoint



(a) Error of Variable Speed

(b) Error of Constant Speed

Fig. 20. Random Waypoint Error

within one nodes transmission range. This data was also plotted and as was the case with the random walk model, all plots were the same irrespective of the total number of nodes in the simulation. The two speed variations in the simulations resulted in very similar plots as well.

The data from the simulation was plotted with the analytical model and can be seen in Figure 19. The random waypoint simulation data and the analytical model are very similar in shape. There are a few slight variations that can be seen in the figure and these can be attributed to the approximation of the area under the spatial density used in the calculation of the analytical model. The random waypoint analytical model proves to be much more accurate than the uniform model in the higher regions of  $r$ . The two are very similar in the lower regions of  $r$ .

Figures 20(a) and 20(b) show the RWP model and uniform model error as compared to the simulated data. The random waypoint model has a confidence level of greater than 90% for  $\frac{L}{2} < r$ . The error is greater below  $\frac{L}{2}$  and is attributed to the lower overall connectivity in these ranges. A slight deviation in the percent of nodes in range for a low value already equates to an unfairly large percentage of error. Simulations themselves can and do vary by a small amount due to the randomness of their behavior. Regardless of the unfair percentage of error analysis, this model is a very reasonable estimate of the random walk mobility model's effective coverage.

## VII. CONCLUSION

In this paper we have shown that the location and transmission range of a mobile node can have a considerable effect on expected node connectivity and density. We presented a mathematical model to predict the behavior of node coverage. The model was extended to the random walk and random waypoint

mobility models and examined for accuracy in each. It was shown that as the transmission range,  $r$ , of a node is increased, the effective mean coverage also increases, but not in a uniform manner. Extensive simulations were conducted to verify these mathematical findings and to demonstrate the importance of the boundary effect.

Future work for effective coverage includes adaptations to additional mobility models, including group mobility models. In addition to adaptations, further refining the spatial node density of the random waypoint model could reduce the variations between the simulated and analytical results. Likewise, comparisons between the presented analytical models, simulated data and real world data could provide extremely useful to the research community.

## REFERENCES

- [1] Bai, F., Sadagopan, N., Krishnamachari, B.: Modeling path duration distributions in manets and their impact on reactive routing protocols. *IEEE Journal on Selected Areas in Communications*. Vol. 22(7), 1357–1373. December (2004)
- [2] Bettstetter, C., Wagner, C.: The Spatial Node Distribution of the Random Waypoint Model. *Proc. First German Workshop Mobile Ad Hoc Networks (MWAM)*. 41–58. March (2002)
- [3] Bettstetter, C.: On the Connectivity of Wireless Multihop Networks with Homogeneous and Inhomogeneous Range Assignment. *VTC'02*. Vol. 3, 1706–1710. September (2002)
- [4] Bettstetter, C., Resta, G., Santi, P.: The Node Distribution of the Random Waypoint Mobility Model for Wireless Ad Hoc Networks. *IEEE Transactions on Mobile Computing*. Vol. 2(3), 257–269. July-Sept (2003)
- [5] Camp T., Boleng, J., Davies, V.: A Survey of Mobility Models for Ad Hoc Network Research. *Wireless Communication & Mobile Computing (WCMC): Special Issue on Mobile Ad Hoc Networking: Research Trends and Applications*. Vol. 2(5), 483–502 (2002)
- [6] Kim, D.S., Hwang, S.K.: Behavioral group mobility model in ad hoc wireless networks. In *9th International Conference on Cellular and Intelligent Communications (CIC2004)*, Seoul. October (2004)
- [7] Kwak, B., Song, N., Miller, L.: A Canonical Measure of Mobility for Mobile Ad Hoc Networks. In *IEEE Military Communications Conference (MILCOM)*. October (2003)
- [8] Lawler, G.F.: *Introduction to Stochastic Processes*. Chapman & Hall. Probability Series. (1995)
- [9] Lin, G., Noubir, G., Rajaraman, R.: Mobility Models for Ad hoc Network Simulation. *Proc. 23rd Conf. of the IEEE Computer and Comm. Soc. (INFOCOM 2004)*. March (2004)
- [10] McDonald, A.B., Znati, T.: A Mobility Based Framework for Adaptive Clustering in Wireless Ad-Hoc Networks. *ieeescomm*. Vol. 17(8). August (1999)
- [11] McDonald, A.B., Znati, T.: A Path Availability Model for Wireless Ad-Hoc Networks. In *Proceedings of the IEEE Wireless Communications and Networking Conference*. 35–40. September (1999)
- [12] Navidi, W., Camp, T.: Stationary Distributions for the Random Waypoint Mobility Model. *IEEE Transactions on Mobile Computing*. Vol. 3(1), 99–108. (2004)
- [13] Resta, G., Santi, P.: An Analysis of the Node Spatial Distribution of the Random Waypoint Mobility Model for Ad Hoc Networks. *Proc. on the Second ACM International Workshop on Principles of Mobile Computing*. 44–50. (2000)
- [14] Royer, E., Melliar-Smith, P., Moser, L.: An Analysis of the Optimum Node Density for Ad hoc Mobile Networks. In *IEEE International Conference on Communications*. June (2001)
- [15] Yoon, J., Liu, M., Noble, B.: Random Waypoint Considered Harmful. *Proc. 21st Ann. Joint Conf. IEEE Computer and Comm. Soc. (INFOCOM 2003)*. 1312–1321. April (2003)
- [16] Zonoozi, M., Dassanayake, P.: User mobility modeling and characterization of mobility patterns. *IEEE Journal on Selected Areas in Communications*. Vol. 15(7), 1239–1252. (1997)